PHILOSOPHICAL TRANSACTIONS OF THE ROYAL SOCIETY A MATHEMATICAL, PHYSICAL & ENGINEERING SCIENCES

Quantum Cascade Lasers: New Resonant Tunnelling Light Sources for the Mid-Infrared

F. Capasso, J. Faist, C. Sirtori, D. L. Sivco, J. N. Baillargeon, A. L. Hutchinson and A. Y. Cho

Phil. Trans. R. Soc. Lond. A 1996 **354**, 2463-2467
doi: 10.1098/rsta.1996.0112

Quantum cascade lasers: new resonant tunnelling light sources for the mid-infrared

By F. Capasso, J. Faist, C. Sirtori, D. L. Sivco, J. N. Baillargeon, A. L. Hutchinson and A. Y. Cho

Bell Laboratories, Lucent Technologies, Murray Hill, NJ 07974, USA

Recent results on quantum cascade lasers are reviewed. In these quantum devices based on resonant tunnelling the wavelength can be selected over a broad range of the infrared spectrum using the same heterostructure material by tailoring the active layer thickness. High power room temperature operation at wavelengths of 5 and 8.5 μm has been achieved. These are the first semiconductor lasers to operate at 300 K and above in this wavelength region.

1. Introduction

The quantum cascade (QC) laser is an excellent example of how quantum engineering can be used to design new laser materials and related light sources. It is based on intersubband transitions between excited states of coupled quantum wells and on resonant tunnelling as the pumping mechanism (Capasso *et al.* 1986). The population inversion between the states of the laser transition is designed by tailoring the electron intersubband scattering times (Faist *et al.* 1994). This tailoring of scattering adds an important dimension to quantum engineering of mesoscopic structures. In QC lasers, unlike all other laser sources, the wavelength is determined by quantum confinement, i.e. by the layer thicknesses of the active region rather than by the chemical properties of the material. As such it can be tailored over a very wide range using the same heterostructure material. Since the initial report of QC lasers in 1994 we have demonstrated emission wavelengths in the 4–8.5 μm range using AlInAs/GaInAs heterostructures lattice matched to InP (Faist *et al.* 1995*a*, *b*; Sirtori *et al.* 1996).

2. Vertical transition QC lasers

In the original QC laser design (Faist *et al.* 1994), the width of the luminescence transition is relatively broad (full width at half maximum (FWHM) is 22 meV) due to the interface roughness since electrons traverse several heterointerfaces in the photon emission process (diagonal or photon assisted tunnelling transition). As a consequence the peak gain is reduced. To circumvent this problem we designed the structure of figure 1 where electrons make a vertical radiative transition essentially in the same well (Faist *et al.* 1995*a*). This reduces considerably the width of the gain spectrum (FWHM $\approx$ 10 meV) and therefore the laser threshold current density. To prevent electron escape in the continuum, which is greatly reduced in the case of the diagonal transition, the superlattice of the digitally graded injector is now designed

Phil. Trans. R. Soc. Lond. A (1996) **354**, 2463–2467
Printed in Great Britain

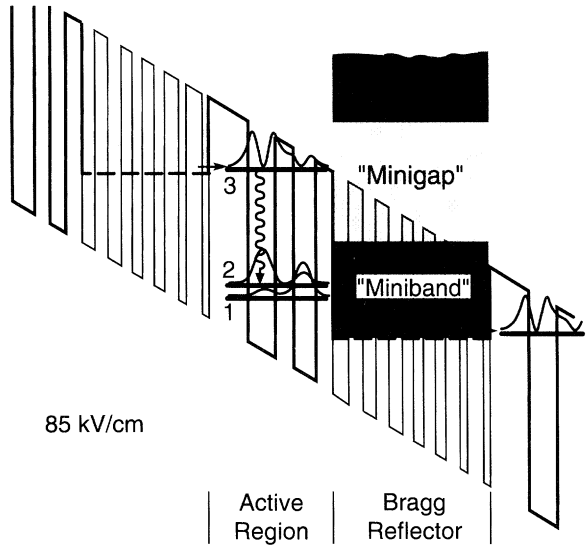

Figure 1. Schematic energy diagram of a portion of the $Ga_{0.47}In_{0.53}As/Al_{0.48}In_{0.52}As$ quantum cascade laser with vertical transition under positive bias condition and an electric field of 8.5×10^4 V cm^{-1}. The dashed lines are the effective conduction band edges of the 20.8 nm thick superlattice electron injector. As shown, this superlattice is also designed as to create a minigap that blocks electron escape from level 3. The wavy line indicates the transition responsible for laser action. The moduli squared of the relevant wavefunctions are shown.

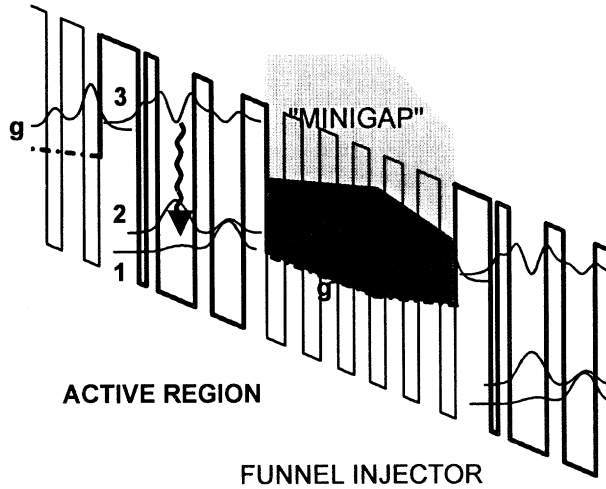

Figure 2. Schematic conduction band diagram of a portion of the active region of a quantum cascade laser with vertical transition and funnel injector under positive bias condition and an electric field of 7.6×10^4 V cm^{-1}. The wavy line indicates the transition responsible for laser action. The moduli squared of the relevant wavefunctions are shown. The layer sequence of one period of the $Al_{0.48}In_{0.52}As/Ga_{0.47}In_{0.53}As$ structure, in nanometers, left to right and starting from the injection barrier is (5.0/0.9), (1.5/4.7), (2.2/4.0), (3.0/2.3), (2.3/2.2), (2.2/2.0), (2.0/2.0), (2.3/1.9), (2.8/1.9). The structures are left undoped, with the exception of layers number 14–16 for sample D-2122 and 11–13 for sample D-2160 which are n-type doped with Si to $N_d = 2 \times 10^{17}$ cm^{-3}.

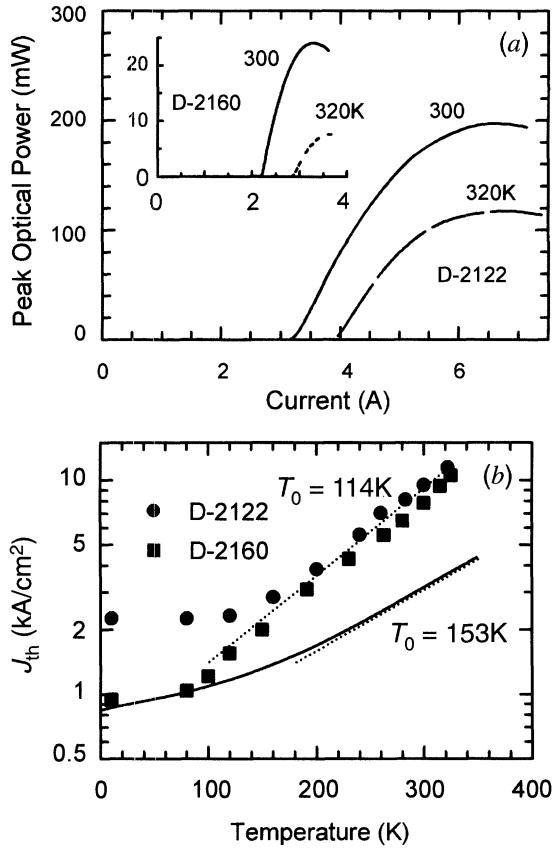

Figure 3. (*a*) Collected pulsed optical power from a single facet versus injection current for heat sink temperatures of $T = 300$ K and $T = 320$ K and for the InP cladded sample D-2122 (dimensions 14 μm×2.9 mm). The collection efficiency is estimated to be $\eta = 70\%$. Inset: same characteristics, but for sample D-2160 (9 μm×3 mm). (*b*) Threshold current density in pulsed operation for both samples as a function of temperature. The solid line is the theoretical prediction. The dotted lines indicate the range over which the T_0 parameter, which describes the exponential dependence of the laser threshold ($\exp T/T_0$), is derived.

as an effective Bragg reflector for electrons in the higher excited state and to simultaneously ensure swift electron escape from the lower states via a miniband facing the latter (figure 1). The active region consists of a 4.5 nm InGaAs quantum well coupled to a 3.6 nm well by a 2.8 nm AlInAs barrier. Tunnelling injection from the superlattice into the active region is through a 6.5 nm AlInAs barrier and electrons escape out of the $n = 1$ state through a 3.0 nm AlInAs barrier. As in the other structure the lower state of the laser transition is separated by an optical phonon (*ca.* 30 meV) from the $n = 1$ state. The calculated relaxation time is $\tau_{21} \approx 0.6$ ps, which is considerably less than that between the $n = 3$ and $n = 2$ state (1.8 ps), thus creating population inversion between these energy levels. Electrons can in turn tunnel out of the $n = 1$ state in a subpicosecond time to prevent electron build-up.

Dramatic performance improvements have been obtained with vertical transition QC lasers. The threshold current density is considerably reduced (by about a factor of 2) leading to higher operating temperatures. In addition, the peak optical power

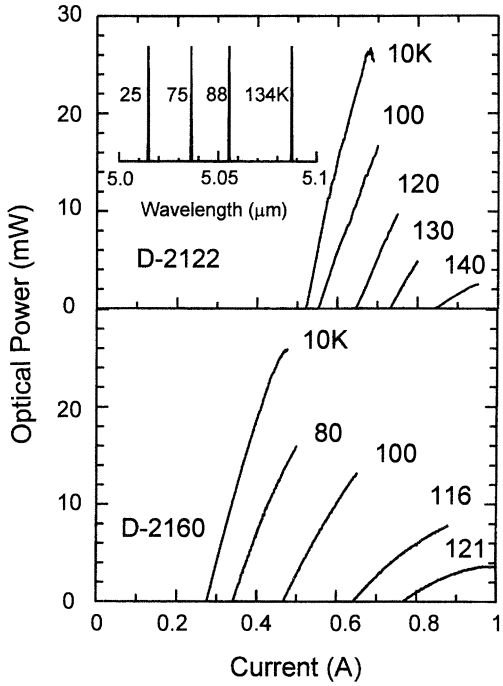

Figure 4. Continuous optical output power from a single facet versus injection current for various heat sink temperatures. (*a*) Sample D-2122 (dimensions 7 μm×2.9 mm). (*b*) Sample D-2160 (9 μm×3 mm). Single mode high resolution spectra are shown in the inset. The side mode suppression ratio is 20 dB.

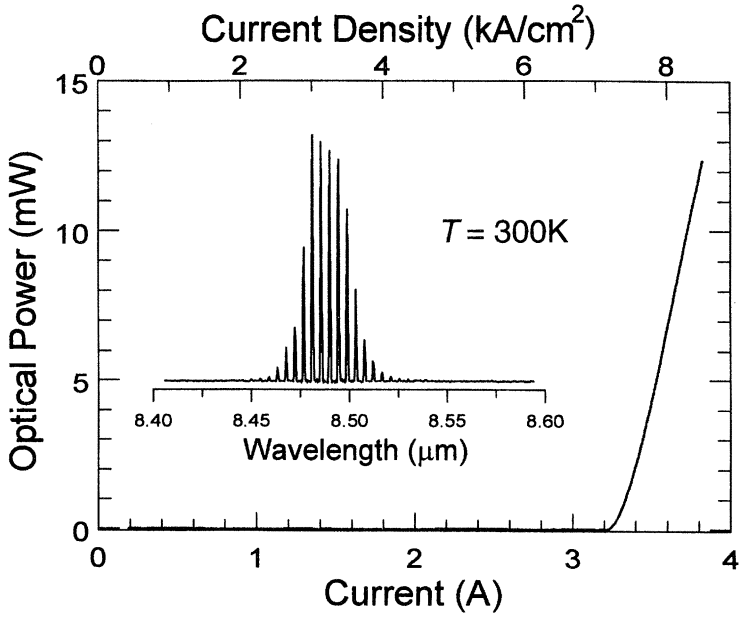

Figure 5. Pulsed characteristics and multimode spectrum at room temperature of quantum cascade laser emitting at $\lambda \approx 8.5$ μm. The maximum peak optical power is 13 mW.

is also greatly enhanced and the lasers can operate in continuous wave at $\lambda \approx 4.5$ μm and $\lambda \approx 8.0$ μm (Faist *et al.* 1995*b*; Sirtori *et al.* 1996).

More recently we have further improved the design of vertical transition QC lasers by adding a thin quantum well between the graded injector layer and the double-well active region (Faist *et al.* 1996) (figure 2). This increases the tunnelling injection efficiency. The above features, together with the substitution of the AlInAs cladding layers with InP regions of much higher thermal conductivity (sample D2122), has led to the room temperature high peak power (*ca.* 200 mW) pulsed operation of QC lasers at $\lambda = 5.2$ μm (figure 3). In sample D2160 the top cladding layer is of AlInAs which leads to lower optical powers at 300 K and above (inset of figure 3). Continuous wave single mode operation has also been achieved up to 140 K (figure 4). We have also recently achieved room temperature pulsed operation at $\lambda \approx 8.5$ μm (figure 5) using a vertical transition QC laser with an energy diagram similar to that of figure 1. For waveguiding the 25 period AlInAs/GaInAs active region was cladded by a top AlInAs layer and by the InP substrate.

The above are the first semiconductor lasers operating at room temperature in the mid-infrared. Their overall performance makes them excellent candidates for many applications such as environmental sensing and pollution monitoring in the 3–5 μm and 8–13 μm atmospheric windows.

In conclusion new light sources (quantum cascade lasers), based on resonant tunnelling, where the population inversion is designed rather than determined by relaxation times intrinsic to the laser material have been reported. For the first time room temperature operation of semiconductor lasers in the 4–8 μm wavelength region has been achieved.

References

Capasso, F., Mohammed, K. & Cho, A. Y. 1986 Resonant tunneling through double barriers, perpendicular quantum transport phenomena in superlattices and their device application. *IEEE J. Quantum Electron.* **QE-22**, 1853–1869.

Faist, J., Capasso, F., Sivco, D. L., Sirtori, C., Hutchinson, A. L. & Cho, A. Y. 1994 Quantum cascade laser. *Science* **264**, 553–556.

Faist, J., Capasso, F., Sirtori, C., Sivco, D. L., Hutchinson, A. L. & Cho, A. Y. 1995*a* Vertical transition quantum cascade laser with Bragg confined excited state. *Appl. Phys. Lett.* **66**, 538–540.

Faist, J., Capasso, F., Sirtori, C., Sivco, D. L., Hutchinson, A. L. & Cho, A. Y. 1995*b* Continuous wave operation of a vertical transition quantum cascade laser above $T = 80$ K. *Appl. Phys. Lett.* **67**, 3057–3059.

Faist, J., Capasso, F., Sirtori, C., Sivco, D. L., Baillargeon, J. N., Hutchinson, A. L., Chu, S. N. G. & Cho, A. Y. 1996 High power mid-infrared ($\lambda \approx 5$ μm) quantum cascade lasers operating above room temperature. *Appl. Phys. Lett.* **68**, 3680–3682.

Sirtori, C., Faist, J., Capasso, F., Sivco, D. L., Hutchinson, A. L., Chu, S. N. G. & Cho, A. Y. 1996 Continuous wave operation of mid-infrared (7.4–8.6 μm) quantum cascade lasers up to 110 K temperature. *Appl. Phys. Lett.* **68**, 1745–1747.

PHILOSOPHICAL TRANSACTIONS OF THE ROYAL SOCIETY A MATHEMATICAL, PHYSICAL & ENGINEERING SCIENCES